# Grassland modeling and monitoring with SPOT-4 VEGETATION instrument during the 1997–1999 SALSA experiment

P. Cayrol [a,*], A. Chehbouni [b], L. Kergoat [c], G. Dedieu [a], P. Mordelet [a], Y. Nouvellon [d]

[a] *CESBIO (CNRS/CNES/UPS), 18 av. E. Belin, bpi 2801, 31401 Toulouse Cedex 4, France*
[b] *IRD/IMADES, Col. San Benito, 83190 Hermosillo, Sonora, Mexico*
[c] *LET (CNRS/UPS), 13 av. col. Roche, BP 4403, 31405 Toulouse Cedex, France*
[d] *USDA-ARS, 2000 E. Allen Road, Tucson, AZ 85719, USA*

## Abstract

A coupled vegetation growth and soil–vegetation–atmosphere transfer (SVAT) model is used in conjunction with data collected in the course of the SALSA program during the 1997–1999 growing seasons in Mexico. The objective is to provide insights on the interactions between grassland dynamics and water and energy budgets. These three years exhibit drastically different precipitation regimes and thus different vegetation growth.

The result of the coupled model showed that for the 3 years, the observed seasonal variation of plant biomass, leaf area index (LAI) are well reproduced by the model. It is also shown that the model simulations of soil moisture, radiative surface temperature and surface fluxes compared fairly well with the observations.

Reflectance data in the red, near infrared, and short wave infrared (SWIR, 1600 nm) bands measured by the VEGETATION sensor onboard SPOT-4 were corrected from atmospheric and directional effects and compared to the observed biomass and LAI during the 1998–1999 seasons. The results of this 'ground to satellite' approach established that the biomass and LAI are linearly related to the satellite reflectances (RED and SWIR), and to vegetation indices (NDVI and SWVI, which is a SWIR-based NDVI). The SWIR and SWVI sensitivity to the amount of plant tissues were similar to the classical RED and NDVI sensitivity, for LAI ranging from 0 and $0.8 \, \mathrm{m^2 \, m^{-2}}$ and biomass ranging from 0 to $120 \, \mathrm{g \, DM \, m^{-2}}$.

Finally, LAI values simulated by the vegetation model were fed into a canopy radiative transfer scheme (a 'model to satellite' approach). Using two leaf optical properties datasets, the computed RED, NIR and SWIR reflectances and vegetation indices (NDVI and SWVI) compared reasonably well with the VEGETATION observations in 1998 and 1999, except for the NIR band and during the senescence period, when the leaf optical properties present a larger uncertainty. We conclude that a physically-sound linkage between the vegetation model and the satellite can be used for red to short wave infrared domain over these grasslands. These different results represent an important step toward using new generation satellite data to control and validate model's simulations at regional scale. © 2000 Published by Elsevier Science B.V.

*Keywords:* SVAT; Grassland; Semi-arid; VEGETATION; SWIR; SALSA

## 1. Introduction

Both natural (floods, fires, droughts, volcanoes, etc.) and human (deforestation, overgrazing, urbanization and pollution) influences are known to cause massive changes in vegetation cover and dynamics. Drastic changes in land surface properties, such as those occurring because of deforestation or the desertification processes are likely to have climatic consequences. There is increasing evidence pointing towards the important role played by land-atmosphere interactions

---

* Corresponding author. Tel.: +33-5-61-55-85-24;
fax: +33-5-61-55-85-00.
*E-mail address:* pascale.cayrol@cesbio.cnes.fr (P. Cayrol).

in controlling regional, continental and global climate. The fluxes of energy, mass and momentum from the land-surface adjust to and alter the state of the atmosphere in contact with land, allowing the potential for feedback at several time and spatial scales. A better understanding of land atmosphere feedback could thus provide answers to questions regarding the climatic implications of land use/cover change, land surface heterogeneity, and of atmospheric composition. Model simulations (Bonan et al. (1992), and Nobre et al. (1991) among others) have shown that drastic changes in vegetation type and cover cause significant impacts on simulated continental-scale climate. Avissar (1995) reviews examples of model and observational evidence showing that regional-scale precipitation patterns are affected by land surface features such as discontinuities in vegetation type. In addition, fluxes of $CO_2$ and other greenhouse gases also depend on the biophysical properties of the land surface. Changes in land cover, land use and climate modify the uptake and release of these gases, leading to changes in their atmospheric concentrations which in turn may influence the global atmospheric circulation.

Plant canopy regulates the exchanges of mass, energy and momentum in the biosphere–atmosphere interface. It dominates the functioning of hydrological processes through modification of interception, infiltration, surface runoff, and its effects on surface albedo, roughness, evapotranspiration, and root system affect soil properties. The amount of vegetation controls the partitioning of incoming solar energy into sensible and latent heat fluxes, and consequently changes in vegetation levels will result in long-term changes in both local and global climates and in turn will affect the vegetation growth as a feedback. In marginal ecosystems, such as arid and semi-arid areas, this may result in persistent drought and desertification, with substantial impacts on the human populations of these regions through reduction in agricultural productivity, reduction in quantity and quality of water supply, and removal of land from human habitability. It is, therefore, scientifically and socially important to study arid ecosystems so that the impact of management practices on the scarce resources can be understood. In this regard, a better understanding of soil–vegetation–atmosphere exchange processes at different time–space scale must be achieved in order

to document the complex interactions between the atmosphere and the biosphere.

During the last decades, vegetation models have been designed to simulate the seasonal and inter-annual variability in plant structure and function. To provide insights on the interaction between terrestrial ecosystems and the atmosphere, some of these vegetation models are now being coupled to soil–vegetation–atmosphere transfer-scheme (SVATs) (e.g. Lo Seen et al., 1997; Calvet et al., 1998a) and even interact with atmospheric models (e.g. to meso-scale model, Pielke et al., 1997; or to GCM, Dickinson et al., 1998). However, the development of process-based models is accompanied by increasing difficulties in obtaining values for the numerous parameters required by the models. This has been pointed out by Gupta et al. (1998) in the case of hydrological models. The vegetation models are also confronted by this calibration problem (e.g. Calvet et al., 1998b). The calibration of these models proves especially difficult and time-consuming when regional and long-term simulations are to be carried out.

In this study, a coupled vegetation growth and SVAT model (V–S model) developed and validated using Hapex–Sahel data (Cayrol et al., in press) has been used to simulate surface radiation, turbulent heat and mass, liquid water and the control of water vapor and $CO_2$ fluxes. Data collected during the semi-arid land–surface–atmosphere (SALSA) program (Goodrich et al., 2000) over grassland site in Mexico during three growing seasons (1997–1999) have been used to assess the performance of the model.

The specific questions addressed in the paper are:

1. Can this coupled model initially developed for the Sahel environment be used in Mexico, and what level of adaptation/calibration is required?
2. Can this model capture the consequences of the observed inter-annual variability of the precipitation in terms of surface fluxes and vegetation development?
3. Is it possible to monitor the surface biophysical parameters using NDVI and/or SWVI as surrogate measures, the 'ground-to-satellite' approach?
4. Can the vegetation growth/SVAT model, when coupled to a radiative transfer scheme, reproduce the seasonal and the inter-annual surface reflectance observed by the VEGETATION sensor, the 'model-to-satellite' approach?

This paper is organized as follows. Section 2 describes both the ground and satellite data sets collected during 1997–1999 seasons. Section 3 presents a brief description of the model and calibration procedure. Section 4 presents an assessment of the performance and robustness of the model. In Section 5, measurements acquired by the new VEGETATION sensor in 1998 and 1999 are also related to biophysical parameters such as green biomass and leaf area index (LAI). Finally, we present a comparison between predicted and observed radiative variables (i.e. reflectances) using VEGETATION sensor. The V–S model was coupled with a radiative transfer model in order to assess its capability to simulate the seasonal variation of visible, near infrared and short wave infrared surface reflectances.

## 2. Site and data description

The study site is located in the upper San Pedro basin (near Zapata village, 110°09′ W; 31°01′ N; elevation 1460 m) and was the focus of the SALSA activities in Mexico during the 1997–1999 field campaigns. The natural vegetation is composed mainly of perennial grasses of which the dominant genus is *Bouteloua*, and the soil is mainly sandy loam (67% of sand and 12% of clay).

### 2.1. Field data

A 7 m tower has been erected in the beginning of 1997 season and equipped with instruments to measure conventional meteorological data (incoming radiation and net radiation at a height of 1.7 m with REBS Q6 net radiometer). The soil heat flux was estimated using six HFT3 plates from REBS Inc., WA, USA. Wind speed and direction, precipitation, air temperature and humidity were also measured. Soil moisture was measured using Time Domain Reflectometry (TDR) sensors (Campbell Scientific CS615 reflectometer) at two locations and four different depths (5, 10, 20 and 30 cm) and a capacity probe (ThetaProbe) which gives an integrated measurement of the water content over the first 5 cm of the soil layer. Radiative surface temperature was measured using Everest Interscience infrared radiometers (IRT) with a 15° field of view at two different viewing angles (0 and 45°). The band pass of these radiometers is nominally 8–14 μm.

Sensible and latent heat fluxes were determined using from the Eddy covariance method. The system is made up of a three-axis sonic anemometer manufactured by Gill Instrument (Solent A1012R) and an IR gas analyzer (LI-COR 6262 model) which is used in a close path mode. The system is controlled by a specially written software, which calculates the surface fluxes of momentum, sensible and latent heat and carbon dioxide. However, during a large part of the experiment, some problems with the LICOR instrumentation did not permit the derivation of latent heat and $CO_2$ fluxes. Therefore, latent heat flux was derived from measurements of sensible heat flux and available energy at the surface as the residual term of the surface energy budget. In 1998, an additional Bowen ratio system has been installed in the same site for a 3 weeks period. Note that the main source of uncertainty concerns the surface soil heat flux. Kustas et al. (1999) showed that uncertainty in soil heat flux is probably larger that the 30% reported in Stannard et al. (1994). Braud et al. (1993) also pointed out the problem associated with the estimation of latent heat flux as the residual term of the energy balance equation given the uncertainty in available energy measurements.

The evolution of the biomass was monitored during the 1997–1999 growing seasons from day of year (DoY) 182–285. The adopted protocol was to cut 10 samples of 1 $m^2$ of biomass along a 100 m transect. Then live phytomass and standing necromass were separated and weighted and the samples were weighted again after 48 h drying at 70°C.

The LAI was determined from biomass and specific leaf area (SLA) measurements (Nouvellon, 1999). In 1998, grass stomatal resistance was measured using two automatic porometers (models MK3 and AP4, Delta T Devices, Ltd, Cambridge, UK).

### 2.2. Satellite data

Two satellite datasets were used to monitor vegetation growth and decay. The first data set consists of daily NOAA/AVHRR images acquired by IMADES (Hermosillo, Mexico) during afternoon overpass from January 1997 to fall 1998. AVHRR red and near infrared top-of-the-atmosphere images were geometrically corrected, re-sampled to 1 km × 1 km resolution, calibrated by IMADES. We also processed daily data acquired since April 1998 around 10:30

Table 1
Listing of the variables, parameters and constants used in the vegetation-SVAT model

| Symbol | Definition | Type |
| --- | --- | --- |
| $a, b$ | Parameters for soil resistance parameterization ($r_{ss}$), $a = 35118$ and $b = 10.517$ (Chanzy, 1991) | Parameter |
| $a_s$ | Coefficient for photosynthates allocation to the shoots compartments (0.53 at $j_1$ and $j_2$, after Nouvellon et al. (2000)) | Parameter |
| $c_g$ | Heat capacity of the soil (DeVries, 1963) | Variable |
| $Ca - \Gamma$ | $CO_2$ concentration gradient between leaf surface and chloroplast ($Ca - \Gamma = 0.640\,\mathrm{g\,CO_2\,m^{-3}}$; Williams and Markley, 1973) | Parameter |
| $C_p$ | Specific heat at constant pressure ($\mathrm{J\,kg^{-1}\,K^{-1}}$) | Constant |
| $C_q$ | Exchange coefficient depends on atmospheric stability | Variable |
| $C_1, C_2, C_3$ | Soil transfer coefficients for moisture (Mahfouf and Noilhan, 1996) | Variable |
| $d$ | Zero plane displacement height for the canopy (m) | Variable |
| $d_n$ | Rate of necromass decays (here, $d_n$ is set to 0.015; Le Roux, 1995) | Parameter |
| $d_1, d_2$ | Depth of surface layer (10 cm), depth of the root zone (40 cm) | Parameter |
| $e_a$ | Vapor pressure at canopy reference height (mbar) | Variable |
| $e_c, e_g$ | Canopy (0.98) and ground surface (0.96) emissivity (Lo Seen et al., 1997) | Parameter |
| $e_{sat}(T_i)$ | Saturated vapor pressure at temperature $T_i$ (mbar) | Variable |
| $e_0$ | Aerodynamic vapor pressure (mbar) at within-canopy source height | Variable |
| $E_g, E_{tr}$ | Soil evaporation, plant transpiration rates ($\mathrm{kg\,m^{-2}\,s^{-1}}$) | Variable |
| $g_r$ | Growth respiration coefficient for roots ($0.6\,\mathrm{g\,CO_2\,g^{-1}}$ DM; Amthor, 1989) | Parameter |
| $g_s$ | Growth respiration coefficient for shoots ($0.49\,\mathrm{g\,CO_2\,g^{-1}}$ DM; Amthor, 1989; Nouvellon, 1999) compartments | Parameter |
| $G$ | Ground heat flux ($\mathrm{W\,m^{-2}}$) | Variable |
| $h$, height | Vegetation height (cm): $3.52 + 0.0073\,M_s\,(\mathrm{kg\,C\,ha^{-1}}) - 0.000024\,M_s^2(\mathrm{kg\,C\,ha^{-1}})$ | Variable |
| $H, H_c, H_g$ | Total, canopy, soil sensible heat flux ($\mathrm{W\,m^{-2}}$) | Variable |
| $I$ | Photosynthetically active radiation ($\mathrm{W\,m^{-2}}$) | Variable |
| IC | Initial carbon storage ($0.12\,\mathrm{kg\,C\,m^{-2}}$, modified from Le Roux (1995)) | Parameter |
| $I_r$ | PAR level for which $r_r$ equals $2r_{r\,min}$ | Parameter |
| $I_s$ | PAR level for stomata half-closure ($25\,\mathrm{W(PAR)\,m^{-2}}$; Kergoat, 1998) | Parameter |
| $I_0$ | Incoming PAR at the top of the canopy ($\mathrm{W\,m^{-2}}$) | Variable |
| $j_1, j_2$ | Phenological dates: maximum of vegetation, DoY 245 and end of the growing season, DoY 250, respectively (observations in situ) | Parameter |
| $k$ | Von Karman's constant ($\sim$0.4 unitless) | Constant |
| $k_e$ | Extinction coefficient for PAR radiation (0.5 unitless; Kergoat, 1998) | Parameter |
| LAI | Leaf area index ($\mathrm{m^2\,m^{-2}}$) | Variable |
| LE, $LE_c$, $Le_g$ | Total, canopy, soil latent heat flux ($\mathrm{W\,m^{-2}}$) | Variable |
| $m_s, m_r$ | Rate of maintenance respiration for shoots and roots | Variable |
| $m_{s0}, m_{r0}$ | Maintenance respiration rate for shoots (0.003 per day) and roots (0.0012 per day), after Amthor (1989) | Parameter |
| $M_s, M_r, M_n$ | Shoots biomass, roots biomass, standing necromass ($\mathrm{kg\,C\,m^{-2}}$) | Variable |
| $n$ | Attenuation coefficient of eddy diffusivity within the vegetation (2.5 unitless, Shuttleworth and Gurney, 1990) | Parameter |
| $n'$ | Attenuation coefficient of wind speed within the vegetation (2.5 unitless, Shuttleworth and Gurney, 1990) | Parameter |
| $P$ | Precipitation reaching the surface ($\mathrm{kg\,m^2\,s^{-1}}$) | Variable |
| $P_c$ | Hourly canopy photosynthesis ($\mathrm{g\,C\,m^{-2}}$) | Variable |
| $P_l$ | Leaf photosynthesis rate ($\mathrm{g\,C\,m^{-2}\,s^{-1}}$) | Variable |
| $P_n$ | Daily canopy photosynthesis ($\mathrm{g\,C\,m^{-2}\,s^{-1}}$) | Variable |
| $Q_{10}$ | Factor for maintenance respiration ($Q_{10} = 2$) | Parameter |
| $r_{aa}{}^{a}$ | Aerodynamic resistance between within-canopy source height and above-canopy reference height ($\mathrm{s\,m^{-1}}$) | Variable |
| $r_{ac}{}^{a}$ | Bulk boundary layer resistance of the canopy ($\mathrm{s\,m^{-1}}$) | Variable |
| $r_{as}{}^{a}$ | Aerodynamic resistance between ground surface (soil source) and within-canopy source height ($\mathrm{s\,m^{-1}}$) | Variable |
| $r_c$ | Canopy resistance ($\mathrm{s\,m^{-1}}$) | Variable |

Table 1 (*Continued*)

| Symbol | Definition | Type |
|---|---|---|
| $r_r$ | Leaf level residual resistance ($s\,m^{-1}$) to $CO_2$ transfer | Variable |
| $r_{r\,min}$ | Minimum residual resistance to $CO_2$ transfer ($137\,s\,m^{-1}$, see Cayrol et al. (in press)) | Parameter |
| $r_s$ | Leaf level stomatal resistance ($s\,m^{-1}$) | Variable |
| $r_s^{CO_2}$ | Leaf stomatal resistance ($s\,m^{-1}$) to $CO_2$ transfer ($r_s^{CO_2} = 1.6 r_s$) | Variable |
| $r_{s\,min}$ | Minimum leaf stomatal resistance ($100\,s\,m^{-1}$, measured in situ) | Parameter |
| $r_{ss}$[a] | Soil surface resistance ($s\,m^{-1}$) | Variable |
| RA, $RA_c$, $RA_g$ | Incoming long-wave radiation, long-wave radiation for the canopy and bare soil, respectively ($W\,m^{-2}$) | Variable |
| Rn, $Rn_c$, $Rn_g$ | Total, canopy and soil net radiation ($W\,m^{-2}$) | Variable |
| $s_s$, $s_r$ | Rate of senescence for the shoots and roots compartments | Variable |
| $s_{s0}$, $s_{r0}$ | Mortality coefficient for shoots (0.01 per day at $j_1$, 0.025 per day at $j_2$, linear interpolated between $j_1$ and $j_2$) and roots (0.01 per day at $j_1$ and $j_2$), best guess modified from Le Roux (1995) | Parameter |
| SLAo | Specific leaf area at $M_s = 0$ ($30\,m^2\,kg\,C^{-1}$, in situ measurements) | Parameter |
| $T$ | Daily average air temperature (K) | Variable |
| $T_a$ | Air temperature at reference height (K) | Variable |
| $T_c$ | Temperature at canopy surface level (K) | Variable |
| $T_g$ | Ground surface temperature (K) | Variable |
| $T_{min}$, $T_{max}$ | Minimum, maximum temperature for photosynthesis (283 and 333 K; Kergoat, 1998) | Parameter |
| $T_r$ | Radiative temperature (K) | Variable |
| Trans | Translocation of carbohydrates ($0.0004\,kg\,C\,m^{-2}$ per day, best guess) | Parameter |
| $T_0$ | Aerodynamic temperature (K) at within-canopy source height | Variable |
| $T_2$ | Deep soil temperature (K) | Variable |
| $u_a$ | Wind speed at reference level $z_{ref}$ ($m\,s^{-1}$) | Variable |
| $u_a$ | Friction velocity ($m\,s^{-1}$) | Variable |
| $u_h$ | Wind speed at the top of the canopy ($m\,s^{-1}$) | Variable |
| vpd | Vapor pressure deficit (Pa) | Variable |
| $w_{eq}$ | Surface soil moisture when gravity balances capillarity forces ($m^3\,m^{-3}$) | Variable |
| $w_{fc}$ | Volumetric soil moisture at field capacity ($0.16\,m^3\,m^{-3}$, see text) | Parameter |
| $w_g$ | Volumetric soil moisture of the surface layer ($m^3\,m^{-3}$) | Variable |
| $w_{sat}$ | Soil moisture at saturation ($0.42\,m^3\,m^{-3}$, estimated from soil texture (clay = 12% and sand = 67%; Cosby et al., 1984) | Parameter |
| $w_{wp}$ | Volumetric soil moisture at wilting point ($0.068\,m^3\,m^{-3}$, see text) | Parameter |
| $w_1$ | Characteristic leaf width (0.005 m; Choudhury and Monteith, 1988) | Parameter |
| $w_2$ | Volumetric soil moisture of the root zone ($m^3\,m^{-3}$) | Variable |
| $z_{ref}$ | Reference height above the canopy where meteorological measurements are available (2 m) | Variable |
| $z_0$ | Roughness length of the canopy (m) | Variable |
| $z_0'$ | Roughness length of the substrate (m) | Variable |
| $\gamma$ | Psychrometric constant ($mbar\,K^{-1}$) | Constant |
| $\lambda_g$, $\lambda_2$ | Ground and deep soil thermal conductivity ($W\,m^{-1}\,K^{-1}$) | Variable |
| $\rho$ | Density of air ($kg\,m^{-3}$) | Constant |
| $\rho_w$ | Density of liquid water ($kg\,m^{-3}$) | Constant |
| $\sigma$ | Stephan–Bolztmann constant ($5.67 \times 10^{-8}\,W\,m^{-2}\,K^{-4}$) | Constant |
| $\sigma_f$ | Screen factor (unitless), $\sigma_f = 1 - \exp(-0.8\,LAI)$ | Variable |
| $\tau$ | Time constant of one day (s) | Constant |
| $\tau_p$ | SVAT time step (s) | Constant |

[a] Resistances formulations can be found in Table 2.

LST by the VEGETATION instrument onboard SPOT-4 (http://sirius-ci.cst.cnes.fr:8080/). VEGETATION is a large field-of-view instrument providing measurements in four spectral bands, namely: blue (0.43–0.47 μm), red (RED, 0.61–0.68 μm), near infrared (NIR, 0.78–0.89 μm) and short wave infrared (SWIR, 1.58–1.75 μm). The resolution is 1 km × 1 km at nadir and is still better than 1.5 km at 50° viewing angle.

We used VEGETATION P-products, which consist of top of the atmosphere reflectance, geometrically corrected and remapped with a multi-temporal and absolute accuracy better than 1 km. A VEGETATION dedicated version of SMAC (Berthelot and Dedieu, unpublished) was used for atmospheric corrections. Water vapor fields at $1 \times 1°$ resolution were derived from atmospheric analyses of the French weather forecast operational model available every 6 h. This procedure for atmospheric correction is now used for the operational processing of VEGETATION data.

VEGETATION and AVHRR sensors have a large field of view, which implies large view zenith angle variations from roughly 0 to $\pm 65°$. The reflectances can vary by factors of two or three, depending on the sun-sensor geometry. This implies that these directional effects have to be corrected. One of the options to minimize these effects is through the use of the so-called vegetation indices. Two vegetation indices were calculated: $NDVI = (NIR − RED/(NIR + RED))$ and $SWVI = (NIR − SWIR)/(NIR + SWIR)$. Normalized reflectance were also computed to remove the effect of surface anisotropy on the VEGETATION data, as described in Appendix A.



Fig. 1. Observed ($\triangledown$, $\bigcirc$ and $\diamondsuit$) and simulated (–, –– and –·) seasonal evolution of the aboveground biomass for years 1997–1999, respectively. Error bars indicate the standard deviation.

## 3. Model description and calibration procedure

### 3.1. Model description

An extensive description of the Vegetation-SVAT model (V–S model) which is used in this study can be found in Cayrol et al. (in press). The mains equations solved by the model are summarized in the Appendix B. Schematically, the vegetation growth model pro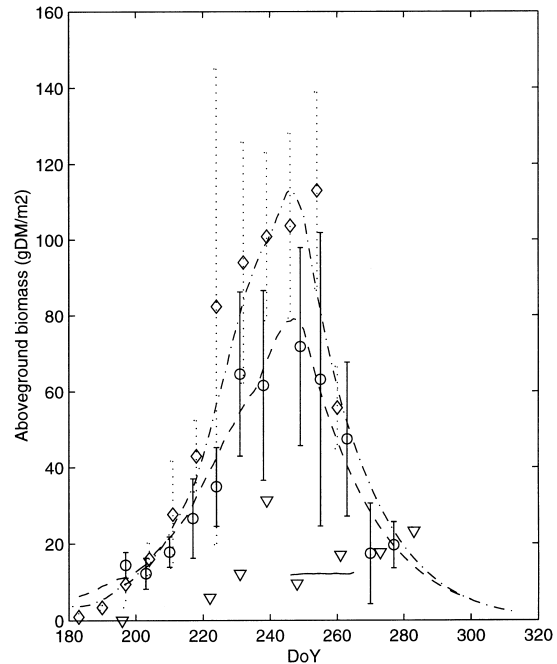vides the LAI, which is then used by the SVAT in the computation of the energy partitioning between soil and the vegetation as well as in the parameterization of turbulent transport and evapotranspiration. This updates the soil water content in the root zone ($w_2$), and thus tissue mortality rate. The stomatal conductance is shared by both sub-models to compute transpiration and photosynthesis.

The surface scheme follows Shuttleworth and Wallace (1985) approach. It considers soil and vegetation as two different sources of latent and sensible heat

Table 2
SVAT resistances formulations

| Formulation[a] | Reference |
| --- | --- |
| $r_{aa}$ $(C_q u_a)^{-1}$ | Mahrt and Ek (1984) |
| $r_{ac}$ $\dfrac{100}{2n' \text{LAI}} \sqrt{\dfrac{w_1}{u_h} \dfrac{1}{1 - \exp(-n'/2)}}$ | Choudhury and Monteith (1988) |
| $r_{as}$ $\dfrac{h \exp(n)}{n K_h} \left[ \exp\left( \dfrac{-nz_0'}{h} \right) - \exp\left( \dfrac{-n(z_0 + d)}{h} \right) \right]$ with $K_h = k u_*(h - d)$ and $u_* = \dfrac{k u_a}{\ln((z_{ref} - d)/z_0)}$ | Shuttleworth and Gurney (1990) |
| $r_{ss}$ $a \exp(-b w_g/w_{sat})$ | Passerat de Silans (1986) |

[a] All the symbols are defined in Table 1.

fluxes. The incoming energy is partitioned between bare soil and vegetation through a screen factor ($\sigma_f$). The dynamic of heat and water flux in the soil is described using the force-restore (Deardorff, 1978). The coefficients involved in the force-restore approach are parameterized as function of soil texture. The original formulation of the force-restore coefficients was modified in order to implicitly describe the vapor phase transfers within the dry soil (i.e. $w_g < w_{wp}$) (Braud

et al., 1993; Giordani et al., 1996), and to represent the gravitational drainage (Mahfouf and Noilhan, 1996).

The four prognostic equations for the SVAT model are numerically solved for the following variables: surface temperature $T_s$, mean surface temperature $T_2$, surface soil volumetric moisture $w_g$, total soil volumetric moisture $w_2$. The three prognostic equations for the vegetation growth model give the evolution of the shoots biomass $M_s$, the root biomass $M_r$ and
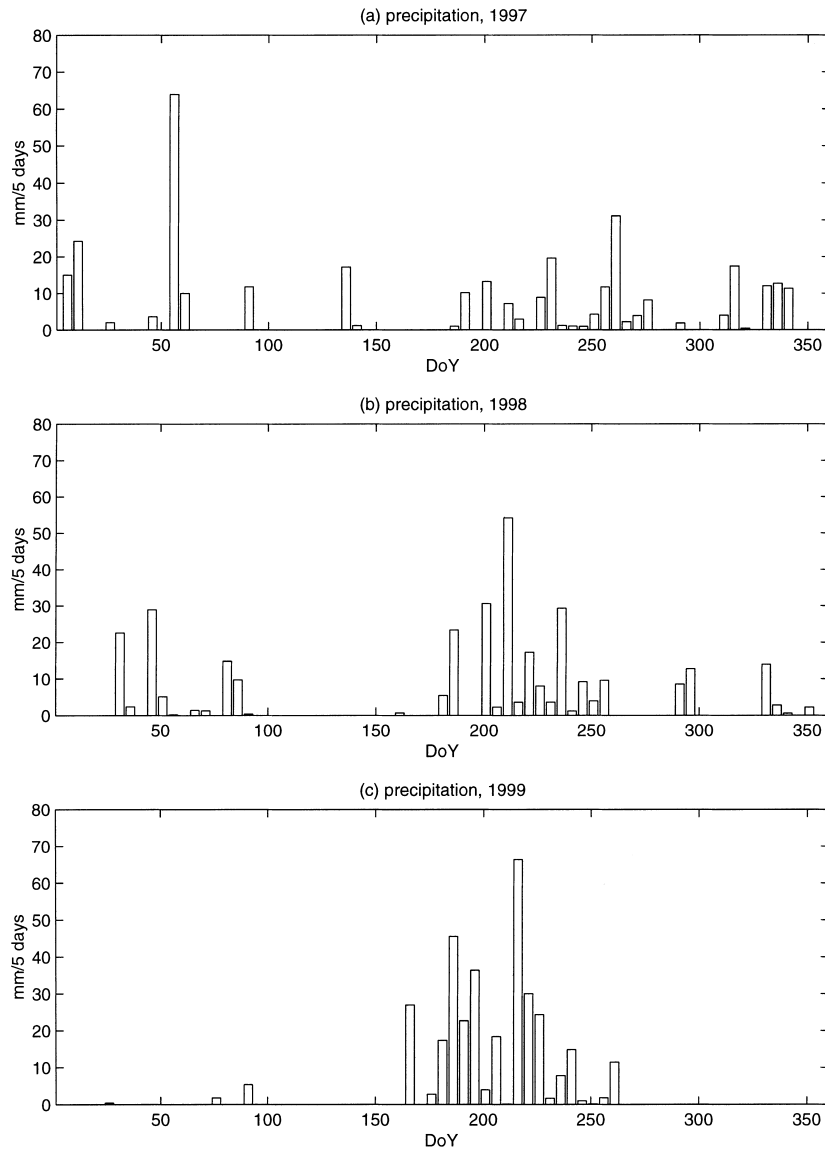


Fig. 2. Precipitation (mm per 5 day) measured on the Zapata grassland site during (a) 1997, (b) 1998 and (c) 1999.

standing necromass $M_n$. The V–S model is driven by meteorological forcing variables, such as, air temperature, air humidity, wind speed, rainfall, and solar radiation. Additional surface characteristics, namely, soil parameters such as soil texture (% clay, % sand), soil thermal and hydraulic properties, root depth; and vegetation parameters such as SLA, maximum rate of photosynthesis are also prescribed (see Table 1).

### 3.2. Choice of the parameters, initialization and calibration

As stated in the introduction, one of our objectives in this study is to investigate the cost in terms of model calibration associated with the adaptation of a model developed and validated over a different site to a new site. A distinction needs to be made between the parameters that can be found in the literature according to soil and/or vegetation classification and those that require on-site calibration.

### 3.2.1. Soil parameters

Several soil parameters are needed in order to specify soil hydrological and thermal properties required by the SVAT model. For the site soil texture, the look-up table of (Clapp and Hornberger, 1978) indicates that the value of the soil moisture at field capacity ($w_{fc}$) and at wilting point ($w_{wp}$) are 0.195 and 0.114 $m^3\,m^{-3}$, respectively. However, the classification of Cosby et al. (1984) indicates that, for this soil type, the wilting point is equal to 0.065 $m^3\,m^{-3}$ and the field capacity is contained between 0.12 and 0.22 $m^3\,m^{-3}$. Schmugge (1980) suggests another relation to estimate the field capacity as a function of soil texture, which leads to over the study site a value of 0.14 $m^3\,m^{-3}$. This value is inconsistent with the values of the maximum observed water content at the root zone in 1999, which represent an indirect way of estimating the soil moisture at the field capacity. In fact, the observed maximum water content is close to 0.18 $m^3\,m^{-3}$ in 1999. Based on the above consideration, an average value of 0.16 $m^3\,m^{-3}$ for $w_{fc}$ and of 0.065 $m^3\,m^{-3}$ for $w_{wp}$ was adopted in this study. Concerning thermal conductivity, the approach described in Van de Griend and O'Neill (1986) has been implemented into the model.

The model also requires appropriate coefficients for the soil resistance parameterization (Tables 1 and 2). In this regard, Chanzy, 1991 reported some difficulties

in establishing a one-to-one relationship between soil moisture and soil resistance to evaporation, even for a single soil type.

### 3.2.2. Surface and plant parameters

According to the measurements made by Nouvellon (1999) over the same site, 80–90% of root biomass is found in the first 30 cm of the soil. Measured average minimal stomatal resistance and specific leaf area ($SLA_0$) were 100 $s\,m^{-1}$ and 30 $m^2\,kg\,C^{-1}$, respectively. Finally, the two phenological stages, $j_1$ and $j_2$ (i.e. growth and senescence timing) have been estimated from the dynamics of the measurements of biomass in 1998 (see Table 1). The growth respiration coefficient for the above ground biomass was set to 0.49 $g\,CO_2\,g^{-1}\,DM$.

The model's initialization depends on the initial amount of carbohydrate in the storage pool, and also on the rate at which this carbon is injected into the shoot and root compartments (initial carbon storage (IC) and Trans in Table 1). Since meteorological data during the first parts of the growing seasons were not
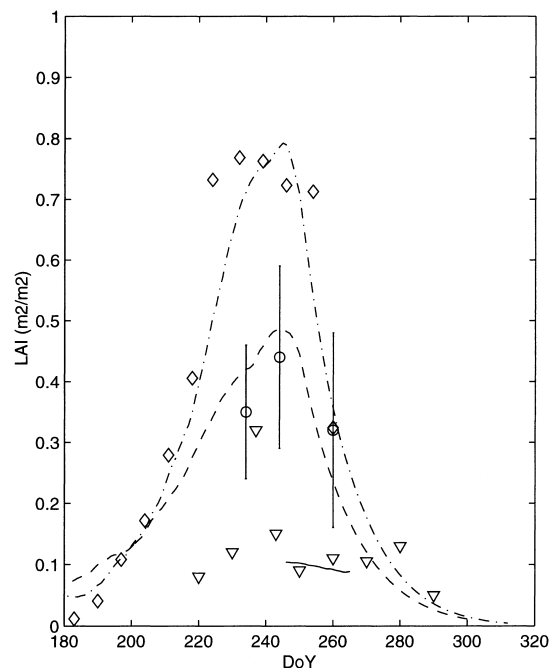


Fig. 3. Observed ($\triangledown$, $\bigcirc$ and $\diamondsuit$) and simulated (–, – – and – ·) seasonal evolution of the LAI for years 1997–1999, respectively. Error bars indicate the standard deviation.

available, the model shoot carbon content had to be initialized so as to match the biomass field measurements on the first day of the simulations for 1997–1999.

## 4. Assessment of the model performance

The V–S model has been run with measured atmospheric forcing variables in conjunction with the parameters described in the previous section and in Tables 1 and 2. Fig. 1 shows the comparison between observed and simulated aboveground biomass during the 1997–1999 growing seasons, respectively. This figure indicates that the biomass simulations closely follow the measurements. As can be seen in the precipitation data presented in Fig. 2a–c the 1999 growing season (Fig. 2c) was much wetter than the 1998 and 1997 growing seasons (Fig. 2a and b).
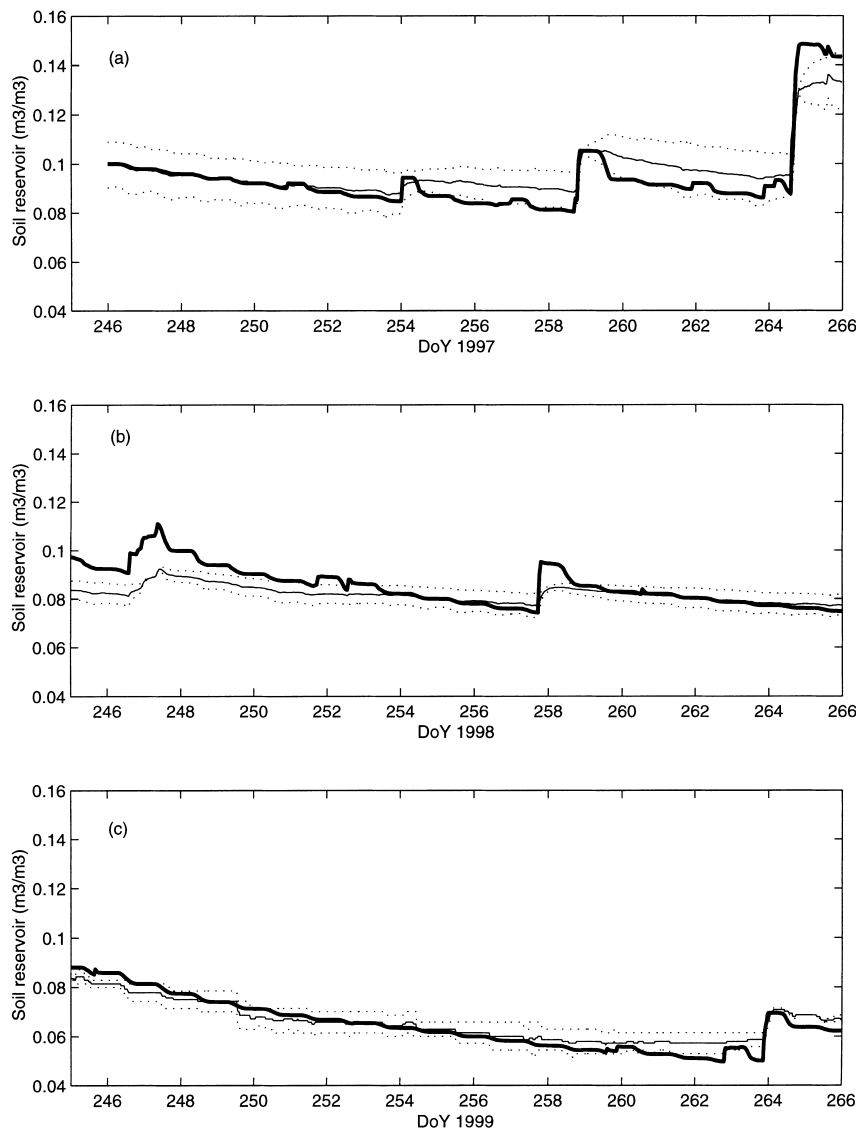


Fig. 4. Observed (–) and simulated ($\cdot$) hourly and half-hourly volumetric soil moisture in the root zone (m$^3$/m$^3$) for a 20-day period in 1997 (a), in 1998 (b) and in 1999 (c), respectively. The two time series of soil moisture measurements are plotted ($\cdots$).

From June to August, total rainfall in 1997 was about 127 mm while it was about 201 mm in 1998 and 304 mm in 1999. As a result, the biomass production was very low in 1997, average in 1998 and high in 1999. The peak biomass only reached 32 g DM m$^{-2}$ in 1997 while it reached 72 g DM m$^{-2}$ in 1998 and 113 g DM m$^{-2}$ in 1999. The days corresponding to

the maximum biomass were different in 1997 when compared to 1998 and 1999. This is due to differences in both the amount and the temporal distribution of the rainfall. Fig. 3 presents a comparison between observed and simulated LAI. The LAI simulated by the V–S model agrees well with the measurements, although the comparison is meaningless for 1997 due to
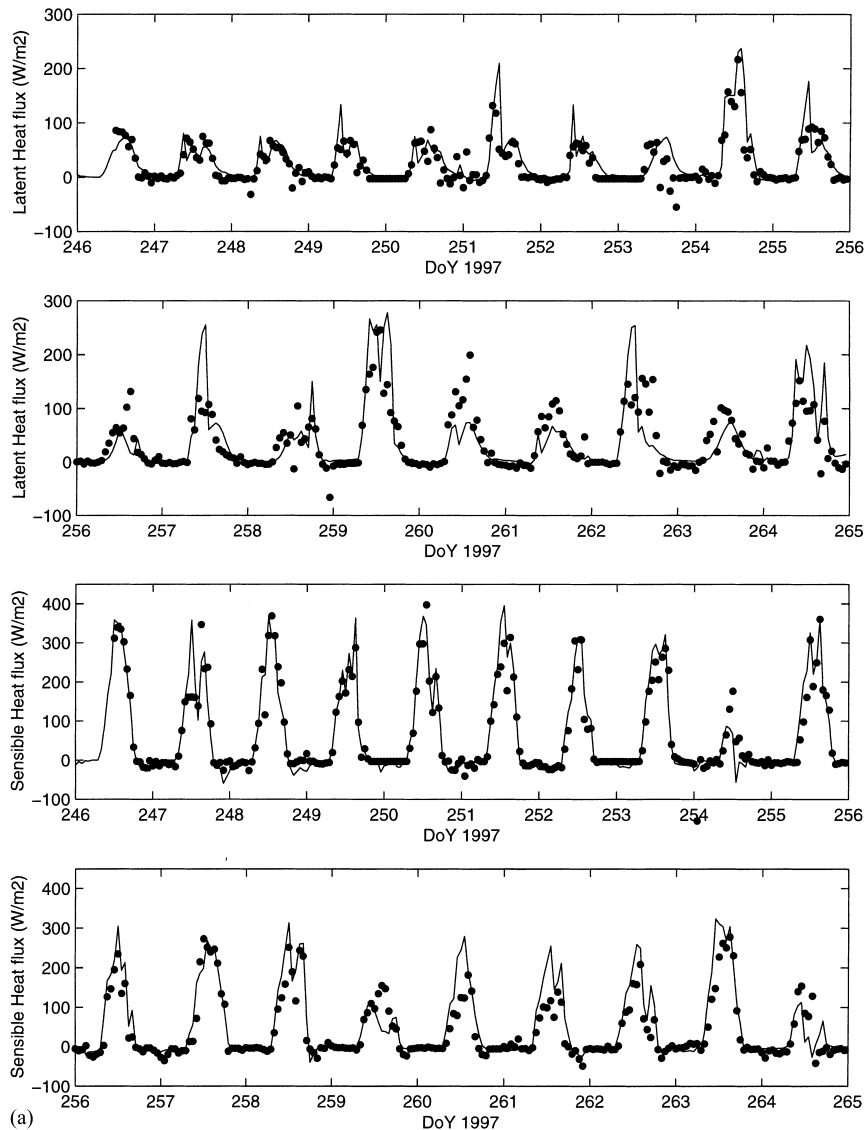


Fig. 5. (a) Simulated (–) and observed (●) hourly latent and sensible heat fluxes for a 20-day period of the 1997 growing season; (b) average diurnal cycle (local solar time) of the difference between measured and simulated components of the energy budget for the 1997 and 1998 growing seasons. Net radiation (– ·), soil heat flux (· · ·), latent heat flux (–) and sensible heat flux (– –). Measurements of sensible and latent heat fluxes were not available for 1998.
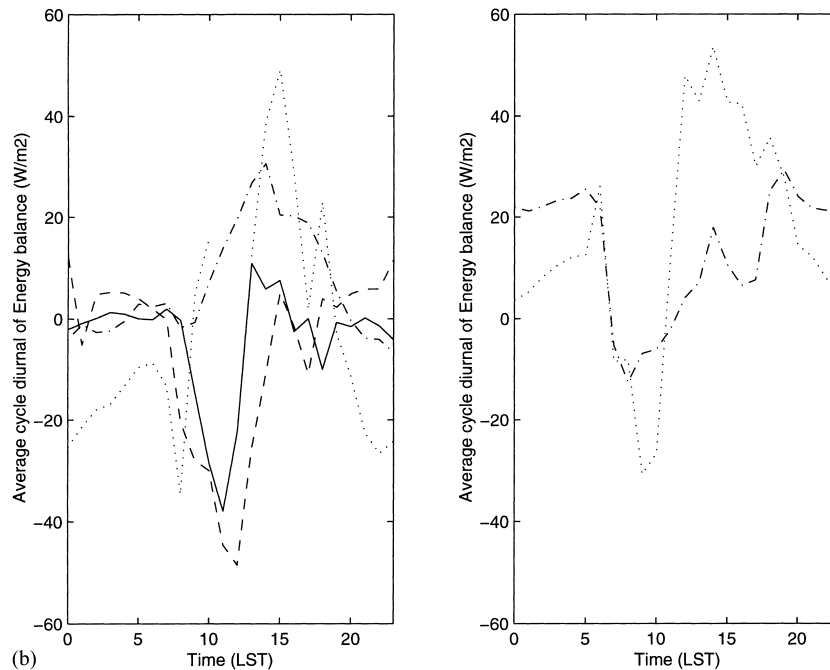
(b)

Fig. 5 (*Continued*)

the short observation period. Maximum LAI was 0.32 in 1997, but it reached 0.4 in 1998 and 0.75 in 1999.

Fig. 4 focuses on a 20-day period (day of year 246–265), and shows the dynamics of the simulated and observed hourly values (half hourly for 1999) of soil moisture in the root zone ($w_2$) for all three study years. This period corresponds to the end of the rain season, and the grasses are usually at maximum development. The simulated soil moisture is within the range of TDR measurements, except for DoY 246–255 in 1998, when soil moisture is overestimated. This is mainly the result of model's errors, which occur earlier in 1998 (the simulation starts at DoY 171 for this year). Such discrepancies were inherent to the use of the same set of parameters (soil resistance, field capacity). This gives a reasonable agreement for the 3 years, although a year to year re-calibration can produce better but less robust results. The 20-day period corresponds to a dry spell in 1999, although the simulated soil moisture is much higher than in 1997 when averaged over the whole growing season.

The time series of the simulated versus observed latent and sensible heat fluxes are shown in Fig. 5a for the same period of time. The root mean square error

(RMSE) between measured and simulated latent and sensible heat fluxes were 36 and 38 W m$^{-2}$, respectively and therefore in good agreement. On Fig. 5b, we have represented the average diurnal cycle of the difference between the observed and estimated components of the energy balance for 1997 and 1998. There is a systematic bias around 11.00 h (LST) with an overestimation of the simulated latent and sensible heat fluxes. Given the errors associated with surface flux measurements in semi-arid regions, and the quality of the energy balance closure, this bias is relatively small.

Fig. 6a–c present comparison of daytime (7.00 h to 20.00 h) measured and simulated radiative surface temperature (DoY 246–265) in 1997–1999, respectively. The results for the 3 years are rather similar. There is a slight underestimation of the radiative surface temperature for the highest values (>50°C), but the correlations for the whole range of data are strong.

There is still room for validation. For instance, the allocation of carbon to the roots, as well as the partition between soil evaporation and plant transpiration were not measured and validated. Moreover, the simulations also reflect the uncertainties in some critical
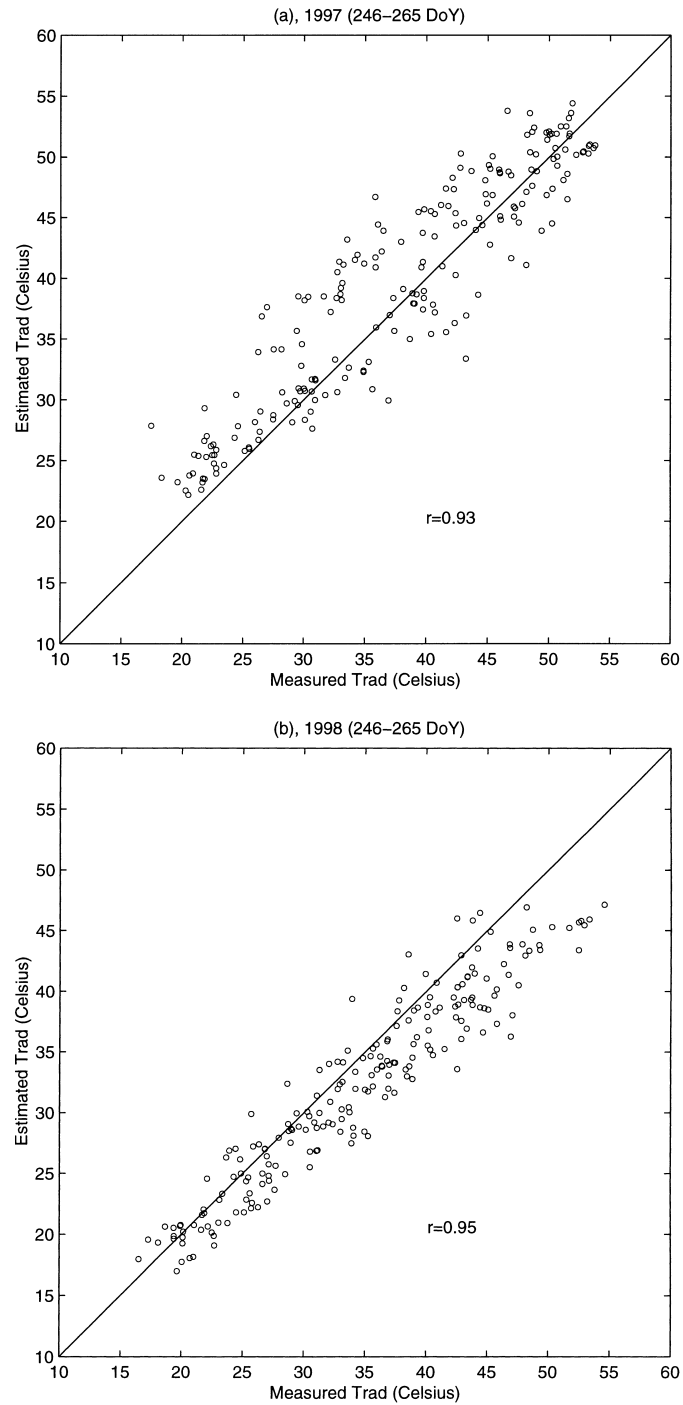
Fig. 6. (a) Simulated radiative temperature vs. ground-based observations at nadir for year 1997, (hourly data, DoY 246–265). The (1:1) line and the correlation coefficient (r) are indicated; (b) same as Fig. 6a, but for year 1998 (DoY 246–265); (c) simulated radiative temperature vs. ground-based observations at nadir for 1999 (half-hourly data, DoY 246–265).
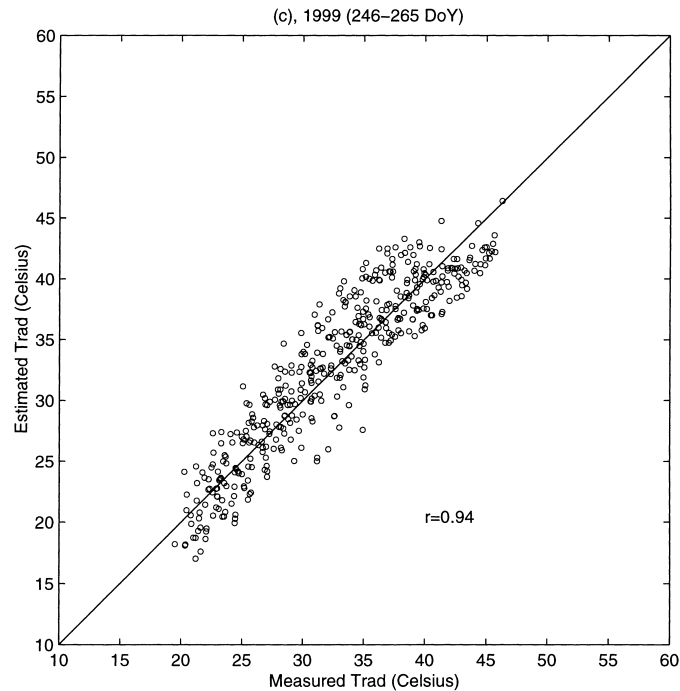
Fig. 6 (*Continued*)

parameters, as highlighted by Cayrol et al. (in press). Nevertheless, the previous evaluations show that the main features of the water and carbon dynamics are properly reproduced by the V–S model, which captures the variability of plant response to the climate variability.

## 5. Ground and satellite data

The objective of this section is to assess the capability of the SPOT4-VEGETATION and NOAA/AVHRR sensors to track the temporal evolution of the vegetation, and to address the questions 3 and 4 mentioned in Section 1.

Both ground measurements and model results presented in the previous section indicate that the LAI of the Zapata grassland site is low (less than 0.8), and strongly variable over the timeframe of the study. Before exploiting the coupling of remotely sensed data and models, we need to verify whether the seasonal evolution as well as the year to year variability of the vegetation is captured by satellite observations, even for such a low vegetation cover.

### 5.1. Ground-to-satellite approach

Fig. 7a–c present the temporal variations of AVHRR and VEGETATION NDVI for the 1997–1999 growing seasons, respectively. The AVHRR NDVI signal in 1997 is almost flat, with a small and late peak near DoY 285, whereas it increases much earlier and reaches higher values in 1998. In 1998, VEGETATION and AVHRR-based NDVI show consistent patterns. These two NDVI time series are not expected to match, because of differences in the spectral bands, instrument field of view and data processing. In 1998 and 1999, the time profiles show similar patterns, with a much more pronounced peak in 1999, which is qualitatively consistent with the biomass data in Figs. 1 and 3.

Fig. 8 presents the seasonal variations of VEGETATION-based surface reflectance during the 1999 season. The strong day-to-day variations reflect the changes in the sun-sensor-target geometry, which affect anisotropic surfaces. In order to compare the surface reflectance to vegetation biophysical properties, these directional effects have been removed, as detailed in Appendix A. This correction minimizes the short term variations and retains the seasonal
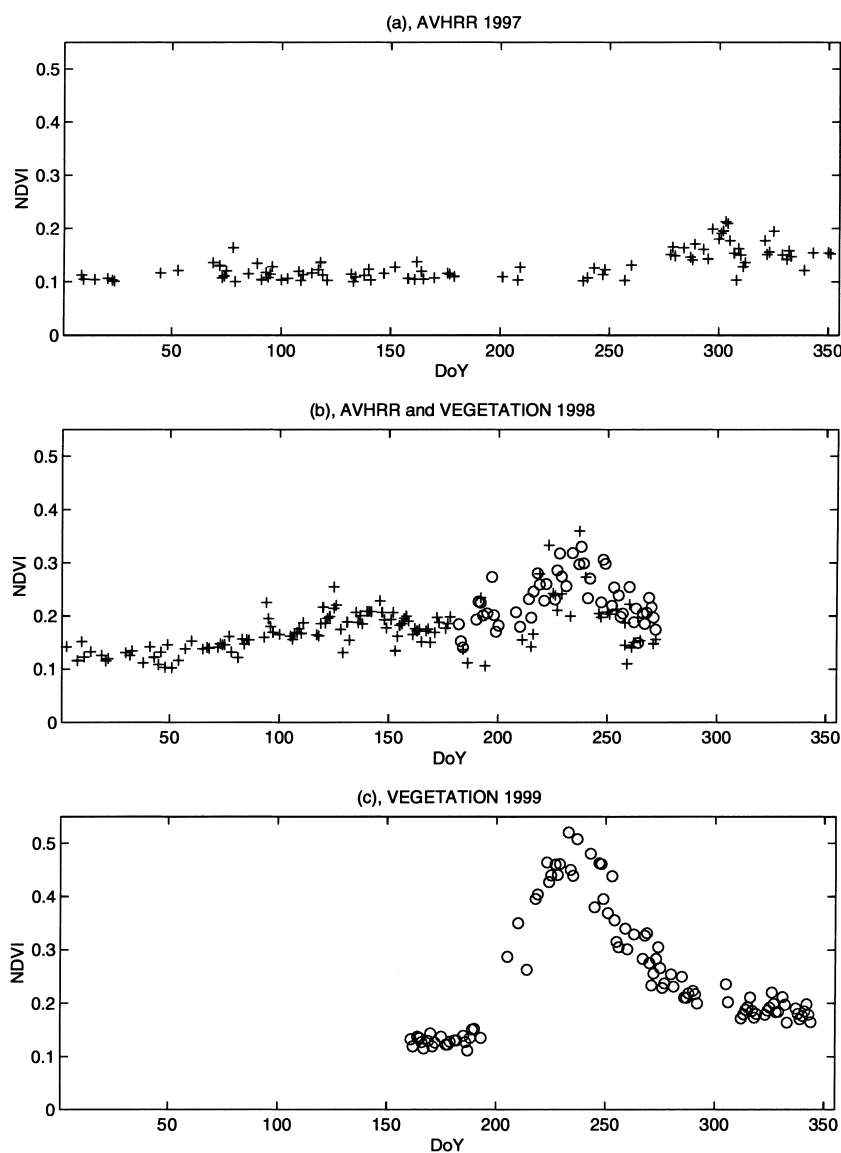
Fig. 7. NDVI time profile over the Zapata grassland, obtained from AVHRR (+) during (a) 1997 and (b) 1998 and from VEGETATION (○) during (b) 1998 and (c) 1999.

evolution. It is the latter corrected surface reflectances, which are used in the subsequent discussion.

The main objective in grassland monitoring is to estimate the evolution with time of the biomass using satellite data as surrogate measures. Scatter plots of LAI and biomass versus the SWIR and the RED reflectance (Fig. 9a and b) reveal significant linear relationships (Table 3). It is well-known that the green leaf

pigments absorb in the red wavelength and that the leaf water absorbs in the SWIR wavelength (e.g. Hunt and Rock, 1989). The figures establish that such relationships are still valid at the satellite and canopy level. This result had still to be demonstrated for the SWIR band. The correlation coefficient of the SWIR/biomass (SWIR/LAI, respectively) is $r = -0.63$ ($r = -0.68$) whereas it is $-0.74$ ($-0.76$) for the RED band. The
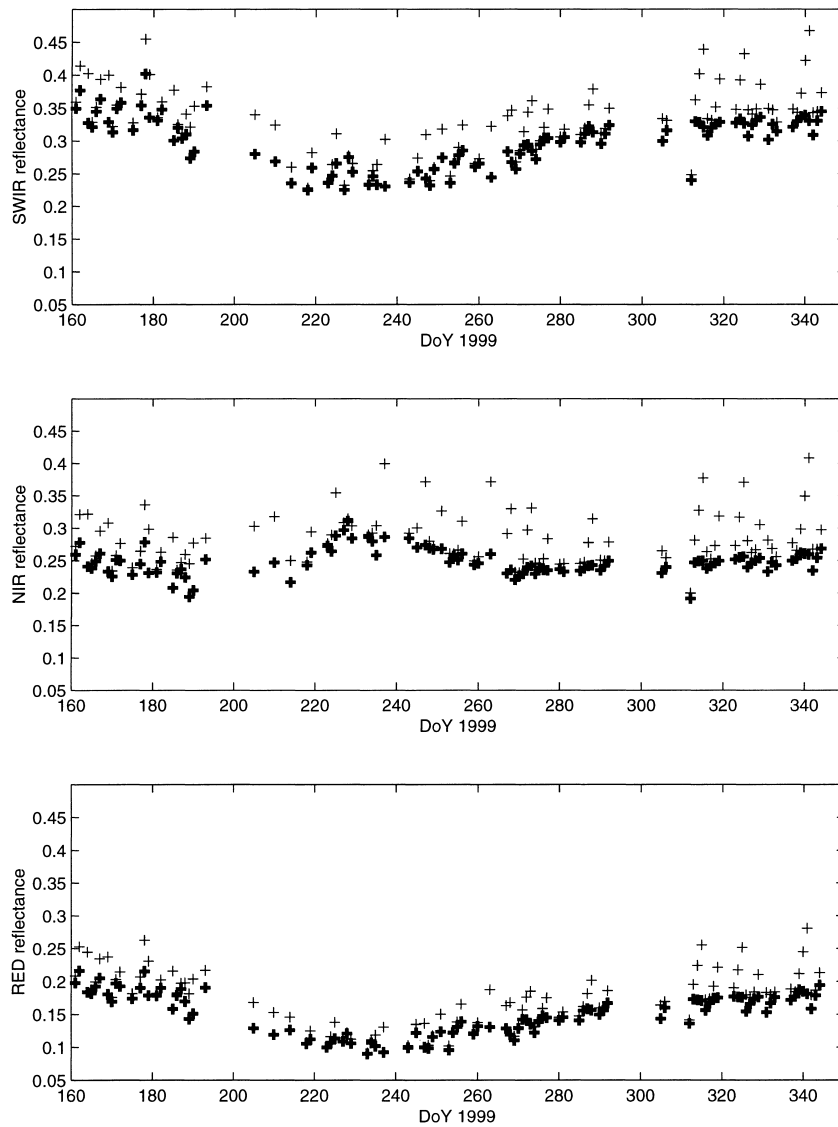
Fig. 8. Summertime reflectance (SWIR, NIR and RED reflectances) acquired by the VEGETATION sensor over the Zapata grassland in 1999. Bold symbols represent reflectances after correction for surface anisotropy effects.

scattering is partly caused by the residual noise, which still impairs the satellite time series. This noise seems to be larger for the SWIR than for the RED band (Fig. 8), and this may be related to the SWIR absorption by the superficial soil moisture during the rain season (DoY 200–250). Another slight difference is that the RED reflectance increases gradually during the senescence period (270–320) whereas the SWIR increases more rapidly and plateaus around DoY 290.

Whether this is related to a different timing in leaf 'drying' and leaf 'yellowing' remains unclear at this stage. When the reflectances are combined into vegetation indices, the correlation improved (Fig. 9c) and reached $r = 0.81$ ($r = 0.88$, respectively) for the NDVI/biomass (NDVI/LAI) and $r = 0.76$ ($r = 0.86$) for the SWVI/biomass (SWVI/LAI, respectively). The results are slightly better when the satellite data acquired during senescence are excluded (black symbols
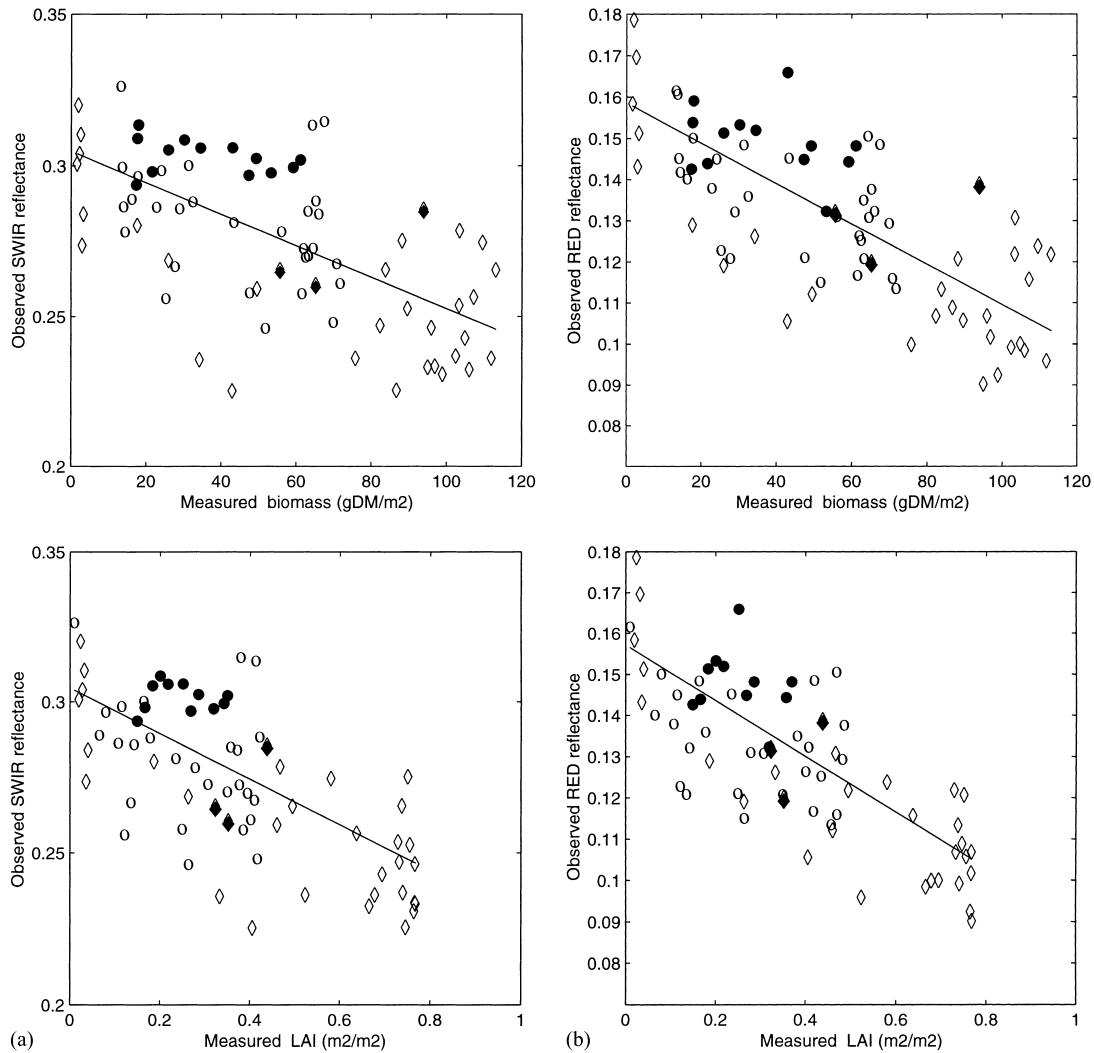
Fig. 9. Scatter diagrams of the SWIR reflectance acquired by the VEGETATION sensor vs. the measured aboveground biomass and LAI during the two growing seasons (○), (◇) and senescence periods (●), (◆) of 1998 and 1999, respectively. The linear regressions are also plotted. Daily 'measurements' of biomass and LAI are linearly interpolated from Figs. 1 and 3; (b) as in Fig. 9a except for the RED reflectance; (c) as in Fig. 9a except for the SWVI and NDVI vegetation indices.

in Fig. 9a–c). Not surprisingly, the regression are better for the LAI than for the biomass.

As far as we know, few studies, if any, have related the seasonal evolution of satellite-measured SWVI and vegetation characteristics, simply because the previous AVHRR sensor did not record the reflectance in the SWIR (AVHRR channel 3 is also sensitive to the thermal emission). While these results are empirical, they are of interest since the impact on aerosol optical depth is much smaller on the SWIR spectral band than on the RED one. Since both wavelengths are sensitive to LAI, it is likely that a combined use of the SWIR, NIR and RED, also available on MODIS, may be more accurate than the former NIR and RED bands alone for vegetation monitoring.

## 5.2. Model-to-satellite approach

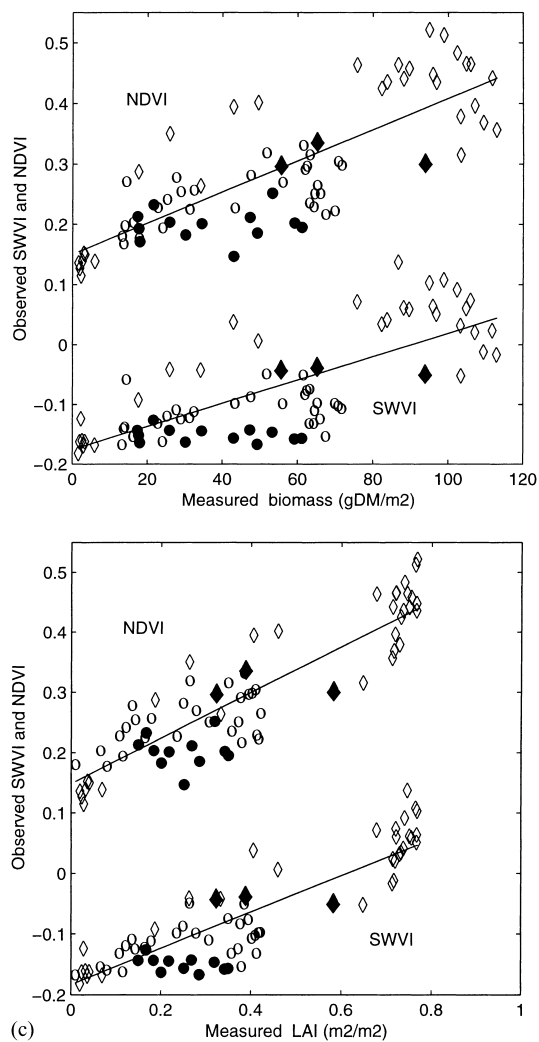Finally, LAI values simulated by the model were used as input to a canopy radiative transfer model

(c)

Fig. 9 (*Continued*)

Table 3
Correlations, slopes and intercepts of the linear relationships between VEGETATION reflectances (SWIR and RED), vegetation indices (SWVI and NDVI) and measured biomass and LAI collected over two years (1998 and 1999)

|  | Biomass (g DM m$^{-2}$)[a] | LAI (m$^2$ m$^{-2}$)[a] |
| --- | --- | --- |
| SWIR | −0.63 | −0.68 |
|  | −0.0005, 0.3048 | −0.0755, 0.3046 |
| RED | −0.74 | −0.76 |
|  | −0.0005, 0.1586 | −0.0677, 0.1572 |
| NDVI | 0.81 | 0.88 |
|  | 0.0026, 0.1505 | 0.3780, 0.1485 |
| SWVI | 0.76 | 0.86 |
|  | 0.0019, −0.1757 | 0.2991, −0.1832 |

[a] Correlation coefficient (*r*), slope and intercept of linear relationships.

(scattering by arbitrarily inclined leaves (SAIL); Ver-hoef, 1984) to compute surface reflectance in RED, NIR and SWIR regions (see Appendix C for more details). The central assumption is that the canopy reflectance depends on variables, green LAI, dead LAI, and can be computed by using SAIL and a set of

fixed parameters such as the green and yellow optical properties, the leaf angle distribution. Two litera-ture datasets provided leaf optical properties for the grasses found on the Zapata site or for closely related species: Asner et al. (1998) and Walter-Shea et al. (1992) (see Table 4). The soil reflectance were derived
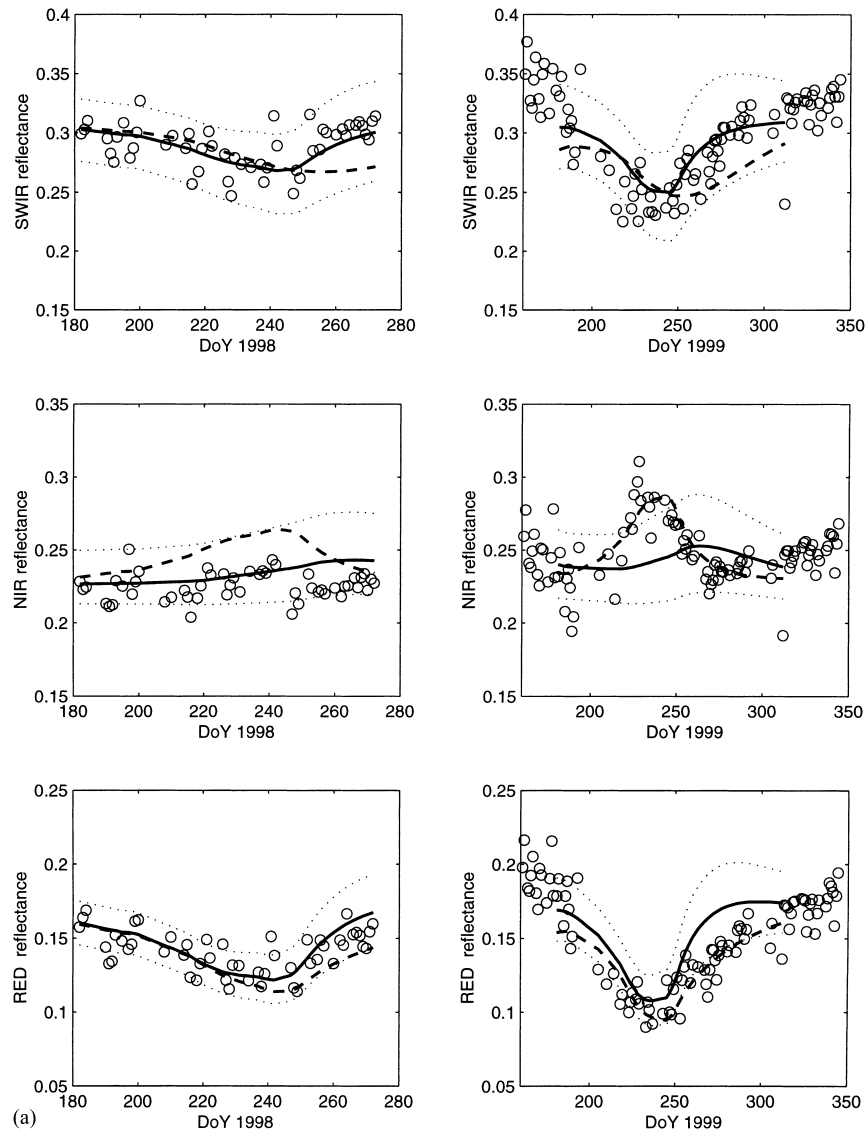


Fig. 10. (a) Comparison of the RED, NIR and SWIR reflectances simulated with the SAIL + V–S model and the normalized VEGETATION reflectances (○) over the Zapata grassland site in 1998 (the three figures on the left) and in 1999 (the three figures on the right). Simulations with the leaf optical properties from Walter-Shea et al. (1992) are in dashed line and solid line represents the simulation with the leaf optical properties from Asner et al. (1998); dotted lines are for the 'bright' and 'dark' parameter sets, see text); (b) as in Fig. 10a except for the vegetation indices, SWVI (○) and NDVI (+).
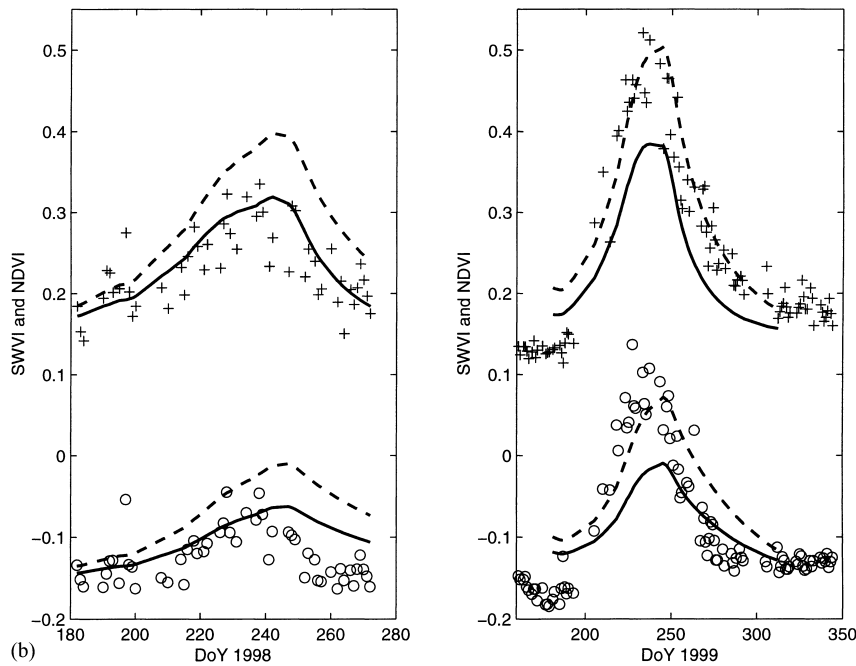
(b)

Fig. 10 (*Continued*)

from springtime VEGETATION data. Simulations errors were assessed by deriving a set of 'bright' optical properties for green, yellow leaves and soil, and a set of 'dark' properties using the standard deviations (Tables 4 and 5). Fig. 10a presents the comparison between simulated and observed reflectances (RED, NIR and SWIR). For each wavelengths, one parameter set or the other yielded a very good match to the VEGETATION data. However, here is no general agreement, because of the difference in the leaf optical properties. This is specially true for the NIR, for which the two simulations exhibit a different temporal pattern in 1999. The first one shows a cycle which is driven by the biomass, whereas the other is driven by the necromass cycle. For the RED and SWIR bands, the 'bright' and 'dark' simulations bracket the data, and the two simulations are similar, although they differ during the senescence period. The poor simulation of the NIR reflectance with the parameter set from Asner et al. (1998) also affects the simulated indices

Table 4
Variability of grass green leaf and litter optical properties in the VEGETATION bands (RED, NIR and SWIR)[a]

| Reflectance | | | Transmittance | | | Reference |
|---|---|---|---|---|---|---|
| RED | NIR | SWIR | RED | NIR | SWIR | |
| *Green leaf* | | | | | | |
| 0.097 (0.02) | 0.38 (0.03) | 0.29 (0.02) | 0.04 (0.08) | 0.34 (0.05) | 0.31 (0.04) | Asner et al. (1998) |
| 0.1 | 0.45 | 0.3 | 0.05 | 0.5 | 0.4 | Walter-Shea et al. (1992) |
| *Litter leaf* | | | | | | |
| 0.43 (0.08) | 0.53 (0.05) | 0.5 (0.08) | 0.13 (0.07) | 0.22 (0.07) | 0.25 (0.08) | Asner et al. (1998) |
| 0.25 | 0.43 | 0.3 | – | – | – | Walter-Shea et al. (1992) |

[a] Mean values from Asner et al. (1998) (standard deviations in parentheses) and mean values from Walter-Shea et al. (1992). The symbol – means no data available.

Table 5
Soil reflectance in the RED, NIR and SWIR bands[a]

| RED | NIR | SWIR |
|---|---|---|
| 0.17 (0.0144) | 0.23 (0.0168) | 0.31 (0.0248) |

[a] Values (standard deviations in parentheses) from VEGETA-TION sensor before the growing 1999 season (DoY 160–175).

in 1999 (Fig. 10b), while the estimations of vegetation indices with the data's Walter–Shea are good. At this stage, the results show that there is a need to have robust estimates of the leaf optical properties, especially for multi-species canopies made of leaves and stems, and during the senescence period. With this caveat in mind, we conclude that the V–S model coupled to the SAIL scheme is able to reproduce the observed satellite reflectances, for the SWIR as well as for the RED and NIR reflectances.

This is an important step towards the use of the new satellite archives (VEGETATION, MODIS) within mechanistic vegetation models.

## 6. Concluding remarks

The first objective of this study was to analyze the capability of coupled Vegetation growth and SVAT models (V–S model) to reproduce the temporal evolution of several variables measured at ground level during three growing seasons in the course of the SALSA program. These variables include grassland biomass and LAI, soil water content and various components of the energy budget. A second objective was to investigate the potential of remotely sensed data to drive or control such a model, within the context of regional scale applications. Four questions, which address these two main objectives have been listed in the introduction. Our conclusions based on the results of our analyses are as follows.

The V–S model used in this study was originally developed for the Sahel environment. Its application to northern Mexico grasslands required some adaptations of the model, not in terms of the processes themselves, but for some of the parameters. For instance, the minimum stomatal resistance, the surface leaf area and the growth respiration rate were different for the SALSA grasses, according to ground measurements and literature survey. Another difference between the Sahelian

annual grasses and the Mexican perennial grasses is the storage capacity of carbohydrate was set to a larger value for the latter. The soil characteristics, especially the water content at wilting point and field capacity were estimated according to Cosby et al. (1984). The use of different classifications, however, produced significantly different estimates, which were not always consistent with the soil moisture measurements. However, the overall functioning including water and $CO_2$ exchanges, was rather similar for the perennial Mexican grasslands and the annual Sahelian grassland, and the V–S model required few changes to simulate the growth, carbon and water balances.

The second question concerns the accuracy of the V–S model outputs. The energy balance and the vegetation growth (biomass, LAI) were reasonably well simulated for the years 1997–1999. This 3-year test was satisfactory for the vegetation sub-model, which captures the large interannual variability, but it was less demanding for the energy sub-model because the intensive observation period was less extensive. The surface radiative temperature was well simulated for the three growing seasons. Overall, it is interesting to note that the V–S model performed relatively well, with the same parameter set, for strongly varying climatic conditions.

The third question deals with the ability of coarse resolution satellite to monitor the seasonal and interannual variability of vegetation status in semi-arid areas. Remotely sensed time series of NDVI and reflectance from the AVHRR and VEGETATION sensors successfully reflected the variability observed in biomass and LAI ground measurements, even for low values of the latter. Since the VEGETATION sensor records the surface short-wave infrared reflectance, individual relationships between LAI or biomass on the one hand, and the SWIR reflectance or a SWIR based vegetation index (SWVI) on the other hand could be established. These relationships were found to be linear for the low values of LAI of the Salsa grasslands. The SWIR and RED bands showed similar sensitivity to biomass and LAI. As a result, the SWIR based SWVI and the classical RED based NDVI produced very similar relationships.

The last question addressed in this study concerns the simulation of the surface radiative signature (RED, NIR and SWIR), with a physically-sound radiative transfer scheme fed by the outputs of the V–S model.

The leaf optical properties were taken from two different dataset. It was shown that the V–S model coupled to the SAIL scheme generally captures the seasonal evolution of the VEGETATION reflectances and spectral indices. For every spectral band, at least one of the input dataset lead to a good simulation of the observed satellite reflectance. However, uncertainties in the leaf optical properties, especially in the green leaf absorption in the NIR and in the dead tissues properties, resulted in large uncertainties in the NIR simulations. Robust estimates of the leaf, stems and litter parameters and of their variability are therefore highly desirable for regional scale applications (e.g. through the validation network of the new sensors like MODIS). From the answers to these different questions, it is concluded that the V–S model is suitable for long term modeling and monitoring of surface processes in arid and semi-arid areas. The physically-based model-to-satellite approach is promising, and the SAIL scheme seems also to be suitable for the SWIR band. Because this spectral domain is known to be less sensitive to most aerosols, the VEGETATION and MODIS datasets may give a different view of the terrestrial ecosystems. Further work will consist in assimilating the satellite measurements at regional scales, with the objective of obtaining accurate simulations of vegetation dynamics and surface energy budget over a large area.

## Appendix A. Correction of the surface anisotropy

To remove the effect of surface anisotropy, we computed a normalized reflectance ($R_{norm}$) using Eq. (A.1) from Wu et al. (1995)

$$R_{norm}(Ao) = R(Aobs) \times F \quad \text{with}$$
$$F = \frac{R_{mod}(Ao)}{R_{mod}(Aobs)} \quad \text{(A.1)}$$

where Ao is the reference or standard sun-sensor geometry (Table 6), Aobs is the actual sun-sensor geometry and $F$ is the factor, which removes the directional effects explained by a BDRF model. The BRDF model used is the AMBRALS model (Wanner et al., 1997) which is based on parameters kernel

$$R_{mod} = k_0 + k_1 f_1(Aobs) + k_2 f_2(Aobs) \quad \text{(A.2)}$$

where $k_0$, $k_1$ and $k_2$ are free parameters obtained fitting $R_{mod}$ to the data, $f_1$ and $f_2$ are the kernels, which are analytical functions of the sun and sensor zenith and azimuth angles. The first kernel aims at reproducing the volume scattering. The second kernel estimates the surface scattering and is based on geometrical approaches. We used the Ross-thick kernel with the Li-sparse kernel. The surface reflectance may then computed for any sun-sensor geometry, e.g.

Table 6
Specification of the SAIL model input parameters

| Canopy structure parameters | |
| --- | --- |
| LAI | As predicted by the V–S model |
| Leaf angle distribution | Spherical (mean leaf angle = 57.30°) |
| *Illumination and view conditions* | |
| Diffuse fraction of solar radiation | 20% |
| *Reference sun-target-sensor*[a] | |
| View zenith angles | 30° |
| Solar zenith angles | 30° |
| Relative azimuth | 140° |

[a] Standard geometry condition of VEGETATION.

the reference geometry (Ao). To account for a seasonal variation of the canopy properties, we used a 'seasonal' Ambral model

$$R_{mod} = Ka_0 + (1 - K)a_0'$$
$$+ (Ka_1 + (1 - K)a_1')f_1(Aobs)$$
$$+ (Ka_2 + (1 - K)a_2')f_2(Aobs) \qquad (A.3)$$

where $a_0$, $a_1$, $a_2$ are the parameters corresponding to the 'maximum vegetation season' and the $a_0'$, $a_1'$, $a_2'$ are the parameters corresponding to the 'minimum vegetation season'. The $K$ coefficient is the NDVI, scaled between 0 and 1. This linear model is fitted to the 1998 and 1999 VEGETATION data and is used to provide normalized seasonal reflectances.

## Appendix B. The V–S model's main equations

Symbols and parameters values are listed in Table 1.

### B.1. Daily time-step

#### B.1.1. Carbon balance
The dynamics of the three carbon compartments is described by a set of three differential equations

$$\frac{dM_s}{dt} = a_s P_n - m_s M_s - Rg_s - s_s M_s \qquad (B.1)$$

$$\frac{dM_r}{dt} = (1 - a_s) P_n - m_r M_r - Rg_r - s_r M_r \qquad (B.2)$$

$$\frac{dM_n}{dt} = s_s M_s - d_n M_n \qquad (B.3)$$

Eq. (B.1) expresses that the daily carbon increment of the shoots is the result of the carbon gain, photosynthesis ($P_n$) minus carbon lost during plant maintenance ($m_s M_s$) and plant growth respiration ($Rg_s$) and carbon losses due to senescence $s_s M_s$. The carbon available for growth is partitioned between the shoot and roots according to the $a_s$ allocation coefficient. The roots obey a similar equation Eq. (B.2), with a symmetric allocation coefficient ($1-a_s$).

The necromass dynamic depends on the difference between necromass production, which is equal to the shoot senescence $s_s M_s$, and necromass decays $d_n M_n$.

The LAI is computed from the shoots biomass and SLA according to a non-linear relationship that accounts for the increasing importance of stems and other non-leaf tissues at high levels of biomass (relationship estimated from measurements Nouvellon, 1999) by the expression

$$SLA = 0.0001[130.4$$
$$-332.5(1 - \exp(-0.0031\text{nbj}))] \qquad (B.4)$$

where nbj is the number of day after the beginning of the growing season.

The carbon balance equations Eqs. (B.1)–(B.3) are solved on a daily basis, where as the photosynthesis ($P_n$) is computed and accumulated on an hourly basis. Indeed, it depends on the stomatal resistance, which is also involved in the SVAT model, and computed on an hourly (or half-hourly) basis.

#### B.1.2. Respiration and senescence
Following McCree (1970) and Amthor (1986, 1989) the total respiration consists of maintenance and growth respiration. The maintenance respiration is proportional to the biomass and its rate ($m_s$ or $m_r$ in Eqs. (B.1) and (B.2)) depends on air temperature according to a classical $Q_{10}$ relationship:

$$m_s = m_{s0} Q_{10}^{T/10} \qquad (B.5)$$

where $T$ is the daily average air temperature and $m_{s0}$ is the respiration rate at 0°C for the shoot ($m_{r0}$ for roots, respectively). The growth respiration is proportional to the amount of new tissue and therefore Eqs. (B.1) and (B.2) have to be rearranged as follows:

$$\frac{dM_s}{dt} = \frac{1}{1 + g_s}(a_s P_n - m_s M_s) - s_s M_s \qquad (B.6)$$

$$\frac{dM_r}{dt} = \frac{1}{1 + g_r}[(1 - a_s) P_n - m_r M_r] - s_r M_r \qquad (B.7)$$

The dry matter is lost through the senescence of shoot and root tissues Eqs. (B.6) and (B.7). We considered here a normal senescence rate $s_{s0}$ ($s_{r0}$ for roots, respectively) and a water stress effect that increases senescence

$$s_s M_s = s_{s0}\left[1 + \left(1 - \frac{w_2 - w_{wp}}{w_{fc} - w_{wp}}\right)\right] M_s \qquad (B.8)$$

## B.2. Hourly (or half hourly) time step

### B.2.1. Stomatal resistance

The leaf stomatal resistance is of Jarvis's (1976) type

$$
\begin{aligned}
r_s &= r_{s\,min} f(I) g(W) h(vpd) \\
&= r_{s\,min} \left( \frac{I_s + I}{I} \right) \left( \frac{w_{fc} - w_{wp}}{w_2 - w_{wp}} \right) \left( \frac{4000 - 1000}{4000 - vpd} \right)
\end{aligned}
$$

(B.9)

### B.2.2. Photosynthesis

At leaf level, $P_l = (Ca - \Gamma)/(r_s^{CO_2} + r_r)$ where $r_s^{CO_2}$ and $r_r$ are the stomatal and residual resistances (i.e. mesophyll diffusion and carboxylation resistances) to $CO_2$ transfer (e.g. Running and Coughlan, 1988). See Cayrol et al. (in press) for parameters derivations.

$$
\begin{aligned}
r_r &= r_{r\,min} g_1(I) g_2(T) \\
&= r_{r\,min} \frac{I_r + I}{I} \frac{(T_{max} - T_{min})^2}{4(T_{max} - T)(T - T_{min})}
\end{aligned}
$$

(B.10a)

At the canopy level, $P_c = \dfrac{\tau(Ca - \Gamma)}{k_e(r'_s + r'_r)} \ln$

$$
\times \left( \frac{r'_s I_s + r'_r I_r + k_e I_0(r'_s + r'_r)}{r'_s I_s + r'_r I_r + k_e I_0(r'_s + r'_r) \exp(-k_e LAI)} \right)
$$

(B.10b)

where $r'_s$ is for $r_{s\,min} g(W) h(vpd)$ and $r'_r$ is for $r_{r\,min} g_2(T)$.

### B.2.3. Prognostic equations, surface fluxes and radiative temperature

The equations giving the evolution of the prognostic variables are

$$
\frac{\partial T_g}{\partial t} = \frac{2\pi^{1/2} G}{(c_g \lambda_g \tau)^{1/2}} - \frac{2\pi}{\tau}(T_g - T_2)
$$

(B.11)

$$
\frac{\partial T_2}{\partial t} = \frac{G}{(356 c_g \lambda_2 \tau)^{1/2}}
$$

(B.12)

$$
\frac{\partial w_g}{\partial t} = \frac{C_1}{\rho_w d_1}(P - E_g) - \frac{C_2}{\tau}(w_g - w_{eq}),
$$
$$
0 \le w_g \le w_{sat}
$$

(B.13)

$$
\begin{aligned}
\frac{\partial w_2}{\partial t} &= \frac{1}{\rho_w d_2}(P - E_g - E_{tr}) \\
&\quad - \frac{C_3}{d_2 \tau} \max[0, (w_2 - w_{fc})], \quad 0 \le w_2 \le w_{sat}
\end{aligned}
$$

(B.14)

The energy balance is written separately for the soil and vegetation

$$
Rn_g - LE_g - H_g - G = 0
$$

(B.15)

and

$$
Rn_c - LE_c - H_c = 0
$$

(B.16)

The network of resistances from Shuttleworth and Wallace (1985), between the soil surface, the within-canopy source level and the above-canopy reference level allows to estimate the latent and sensible heat fluxes across differences in vapor pressure and temperature given by

$$
LE = \frac{\rho C_p}{\gamma} \left( \frac{e_0 - e_a}{r_{aa}} \right)
$$

(B.17)

$$
H = \frac{\rho C_p (T_0 - T_a)}{r_{aa}}
$$

(B.18)

for the soil components

$$
LE_g = \frac{\rho C_p}{\gamma} \left( \frac{e_{sat}(T_g) - e_0}{r_{as} + r_{ss}} \right)
$$

(B.19)

$$
H_g = \frac{\rho C_p (T_g - T_0)}{r_{as}}
$$

(B.20)

for the vegetation components

$$
LE_c = \frac{\rho C_p}{\gamma} \left( \frac{e_{sat}(T_c) - e_0}{r_{ac} + r_{sc}} \right)
$$

(B.21)

$$
H_c = \frac{\rho C_p (T_c - T_0)}{r_{ac}}
$$

(B.22)

The radiative temperature is expressed as follows:

$$
Tr = \left[ \frac{(RA - RA_c - RA_g)}{\sigma} \right]^{0.25}
$$

(B.23)

## Appendix C. The SAIL model

SAIL is a turbid medium reflectance model, which considers a homogeneous canopy and uses the

Kubelka–Munk approximation to the radiative transfer equation (Goel, 1988). The model simulates the canopy spectral reflectance from LAI, leaf and soil optical properties, leaf angle distribution, acquisition geometry and diffuse part of the incoming solar radiation. The ratio between leaf size and vegetation height accounts for the hot-spot effect. The green and yellow LAI were predicted daily by the V–S model. The geometric conditions correspond to the acquisition configurations (Table 6). The soil reflectances for visible, near infrared and short wave infrared were estimated from the first images of VEGETATION sensor before the beginning of the growing season (Table 5). Leaf optical parameters (Table 4) were prescribed for visible, near infrared and short wave infrared from Asner et al. (1998) and Walter-Shea et al. (1992). A version of the SAIL model with two layers was used. Green vegetation was assumed to overtop dead leaves.

## References

Amthor, J.S., 1986. Evolution and applicability of a whole plant respiration model. J. Theoritical Biol. 122, 473–490.

Amthor, J.S., 1989. Respiration and Crop Productivity. Springer, New York.

Asner, G.P., Wessman, C.A., Schimel, D.S., Archer, S., 1998. Variability in leaf and litter optical properties: implications for BRDF model inversion using AVHRR, MODIS and MISR, MODIS and MISR. Remote Sens. Environ. 63, 243–257.

Avissar, R., 1995. Recent advances in the presentation of land-atmosphere interactions in general circulation models. Rev. Geophys. 2, 1005–1010.

Bonan, G.B., Pollard, D., Thompson, S.L., 1992. Effects of boreal forest vegetation on global climate. Nature 359, 716–718.

Braud, I., Noilhan, J., Bessemoulin, P., Haverkamp, R., Vauclin, M., 1993. Bare-ground surface heat and water exchanges under dry conditions: observations and parameterization. Boundary Layer Meteorol. 66, 173–200.

Calvet, J.C., Noilhan, J., Rougean, J.L., Bessemoulin, P., Cabelguenne, M., Olioso, A., Wigneron, J.P., 1998a. An interactive vegetation SVAT model tested against data from six contrasting sites. Agric. For. Meteorol. 92, 73–95.

Calvet, J.C., Noilhan, J., Bessemoulin, P., 1998b. Retrieving the root-zone soil moisture or temperature estimates: a feasibility study based on field measurements. J. Appl. Meteorol. 37, 371–386.

Cayrol, P., Kergoat, L., Moulin, S., Dedieu, G., Chehbouni, A., Calibrating a coupled SVAT/vegetation growth model with remotely sensed reflectance and surface temperature. A case study for the HAPEX-Sahel grassland sites. J. Appl. Meteorol., in press.

Chanzy, A., 1991. Modelisation simplifiée de l'évaporation d'un sol nu utilisant l'humidité et la temperature de surface accessibles par télédétection. Thèse de docteur ingénieur agronome de l'Institut National Agronomique Paris-Grignon, France, p. 221.

Choudhury, B.J., Monteith, J.L., 1988. A four layer model for the heat budget of homogeneous land surfaces. Q.J.R. Met. Soc. 114, 373–398.

Clapp, R.B., Hornberger, G.M., 1978. Empirical equations for some soil hydraulic properties. Water Resour. Res. 14 (4), 601–604.

Cosby, B.J., Hornberger, G.M., Clapp, R.B., Ginn, T.R., 1984. A statistical exploration of the relationships of soil moisture characteristics to the physical properties of soils. Water Resour. Res. 20, 682–690.

Deardorff, J.W., 1978. Efficient prediction of ground surface temperature and moisture, with inclusion of a layer of vegetation. J. Geophys. Res. 83, 1889–1903.

DeVries, D.A., 1963. Thermal properties of soils. In: Van Wijk, N.R. (Ed.), Physics of Plant Environment. Holland Publishing, Amsterdam.

Dickinson, R.E., Shaikh, M., Bryant, R., Graumlich, L., 1998. Interactive canopies for a climate model. J. Climate 11, 2823–2836.

Giordani, H., Noilhan, J., Lacarrère, J., Bessemoulin, P., 1996. Modeling the surface processes and the atmospheric boundary layer for semi-arid conditions. Agric. For. Meteorol. 80, 263–287.

Goel, N.S., 1988. Models of vegetation canopy reflectance and their use in estimation of biophysical parameters from reflectance data. Remote Sens. Rev. 4, 1–212.

Goodrich, D.C., Chehbouni, A., Goff, B., MacNish, B., Maddock III, T., Moran, M.S., Shuttleworth, W.J., Williams, D.G., Watts, C., Hipps, L.H., Cooper, D.I., Schieldge, J., Kerr, Y.H., Arias, H., Kirkland, M., Carlos, R., Cayrol, P., Kepner, W., Jones, B., Avissar, R., Begue, A., Bonnefond, J.-M., Boulet, G., Branan, B., Brunel, J.P., Chen, L.C., Clarke, T., Davis, M.R., DeBruin, H., Dedieu, G., Elguero, E., Eichinger, W.E., Everitt, J., Garatuza-Payan, J., Gempko, Gupta, H., Harlow, C., Hartogensis, O., Helfert, M., Holifield, C., Hymer, D., Kahle, A., Keefer, T., Krishnamoorthy, S., Lhomme, J.-P., Lagouarde, J.-P., Lo Seen, D., Laquet, D., Marsett, R., Monteny, B., Ni, W., Nouvellon, Y., Pinker, R.T., Peters, C., Pool, D., Qi, J., Rambal, S., Rodriguez, J., Santiago, F., Sano, E., Schaeffer, S.M., Schulte, S., Scott, R., Shao, X., Snyder, K.A., Sorooshian, S., Unkrich, C.L., Whitaker, M., Yucel, I., 2000. Preface paper to the semi-arid land-surface-atmosphere (SALSA) program special issue. Agric. For. Meteorol. 105, 3–19.

Gupta, H.V., Sorooshian, S., Yapo, P.O., 1998. Toward improved calibration of hydrologic models: multiple and non commensurable measures of information. Water Resour. Res. 34 (4), 751–763.

Hunt Jr., E.R., Rock, B.N., 1989. Detection of changes in leaf water content using near- and middle-infrared reflectances. Remote Sens. Environ. 30, 43–54.

Jarvis, P.G., 1976. The interpretation of the variations in the leaf water potential and stomatal conductance found in canopies in the field. Phil. Trans. R. Soc. London, Ser. B 273, 593–610.

Kergoat, L., 1998. A model for hydrological equilibrium of leaf area index on a global scale. J. Hydrol. 212/213, 268–286.

Kustas, W.P., Prueger, J.H., Humes, K.S., Starks, P.J., 1999. Estimation of surface heat fluxes at field scale using surface

layer versus mixed-layer atmospheric variables with radiometric temperature observations. J. Appl. Meterol. 38, 224–238.

Le Roux, X., 1995. Etude et modélisation des échanges d'eau et d'énergie sol-végétation-atmosphére dans une savane humide (Lamto, Côte d'Ivoire). Thèse de l'université Pierre et Marie Curie, Paris, France, p. 203.

Lo Seen, D., Chehbouni, A., Njoku, E.G., Saatchi, S., Mougin, E., Monteny, B., 1997. A coupled biomass production, water and surface energy balance model for remote sensing application in semiarid grasslands. Agric. For. Meteorol. 83, 49–74.

Mahfouf, J.F., Noilhan, J., 1996. Inclusion of gravitational drainage in a land surface scheme based on the force-restore method. J. Appl. Meteorol. 35 (6), 987–992.

Mahrt, L., Ek, M., 1984. The influence of atmospheric stability on potential evaporation. J. Clim. Appl. Meteorol. 23, 222–234.

McCree, K.J., 1970. An equation for the rate of respiration of white clover plants grown under controlled conditions. In: Setlik, I. (Ed.), Prediction and Measurement of Photosynthetic Productivity. Proceedings of the IBP/PP Technical Meeting, Trebon, PUDOC, Wageningen, The Netherlands, pp. 221–229.

Nobre, C.A., Sellers, P.J., Shukla, J.U., 1991. Amazonian defo-restation and regional climate change. J. Climate 4, 957–987.

Nouvellon, Y., 1999. Modélisation du fonctionnement de prairies semi-arides et assimilation de données radiométriques dans le modèle. Thèse de docteur ingénieur agronome de l'Institut National Agronomique Paris, France.

Nouvellon, Y., Rambal, S., Lo Seen, D., Moran, M.S., Lhomme, J.P., Bégué, A., Chehbouni, A.G., Kerr, Y., 2000. Modelling of daily fluxes of water and carbon from shortgrass steppes. Agric. For. Meteor. 100, 137–153.

Passerat de Silans, A., 1986. Transferts de masse et de chaleur dans un sol stratifié soumis à une exitation atmosphérique naturelle. Comparaison modèle expérience, Thèse de l'institut National de Polytechnique de Grenoble, France, 205 p.

Pielke, R.A., Liston, G.E., Lu, L., Vidale, P.L., Walko, R.L., Kittel, T.G.F., Parton, W.J., Field, C.B., 1997. Coupling of land and atmospheric models over the GCIP area — CENTURY, RAMS, and SIB2C, 2–7 February 1997, LongBeach, CA (preprint of the 13th Conference on Hydrology).

Running, S.W., Coughlan, J.C., 1988. A global model of forest ecosystem processes for regional applications. Hydrological balance canopy gas exchange and primary production processes. Ecol. Model. 42, 125–154.

Schmugge, T.J., 1980. Effect of texture on microwave emission from soils. IEEE Trans. Geosci. Rem. Sensing, GE 18 (4), 353–361.

Shuttleworth, W.J., Gurney, R.J., 1990. Evaporation from sparse crops — an energy combination theory. Q.J.R. Met. Soc. 111, 839–855.

Shuttleworth, W.J., Wallace, J.S., 1985. The theoretical relation-ships between foliage temperature and canopy resistance in sparse crops. Q.J.R. Met. Soc. 116, 497–519.

Stannard, D.I., Blanfort, J.H., Kustas, W.P., Nichols, W.D., Amer, S.A., Shummge, T.J., Weltz, M.A., 1994. Interpretation of surface flux measurements in heterogeneous terrain during the Monsoon'90 experiment. Water Resour. Res. 30, 1227–1239.

Van de Griend, A.A., O'Neill, P.E., 1986. Discrimination of soil hydraulic properties by combined thermal infrared and micro-wave remote sensing. In: Proceedings of the IGARSS'86 Sym-posium, Vol. 254, Zurich, 8–11 September 1986. ESA SP, pp. 839–845.

Verhoef, W., 1984. Light scattering by leaf layers with application to canopy reflectance modeling: the SAIL model. Remote Sens. Environ. 16, 125–141.

Walter-Shea, E.A., Blad, B.L., Hays, C.J., Mesarch, M.A., 1992. Biophysical properties affecting vegetation canopy reflectance and absorbed photosynthetically active radiation at the FIFE site. J. Geophys. Res. 97 (D17), 18925–18934.

Wanner, W., Strahler, A.H., Hu, B., Muller, J.P., Li, X., Barker Schaaf, C.L., Barnsley, M.J., 1997. Global retrieval of bidirec-tional reflectance and albedo over land from EOS MODIS and MISR data: theory and algorithm. J. Geophys. Res. 102, 17143–17161.

Williams, G.J., Markley, J.L., 1973. The photosynthetic pathway type of North American shortgrass prairie species and some ecological implications. Photosynthetica 7 (3), 262–270.

Wu, A., Li, Z., Cilhar, J., 1995. Effects of land cover type and greenness on advanced very high resolution radiometer bidirectional reflectance: analysis and removal. J. Geophys. Res. 100, 9179–9192.